Electronic Supplementary Material (ESI) for Journal of Materials Chemistry A.

Supporting Information

Ultrathin Cobalt-based Zeolitic Imidazolate Framework Nanosheets Array with Strong Synergistic Effect towards Efficient Oxygen Evolution

Junhui Cao[a], Chaojun Lei[a], Jian Yang[a], Xiaodi Cheng[a], Zhongjian Li[a], Bin Yang[a],
Xingwang Zhang[a], Lecheng Lei[a], Yang Hou[a,]*, Kostya (Ken) Ostrikov[b]

[a]Key Laboratory of Biomass Chemical Engineering of Ministry of Education,
College of Chemical and Biological Engineering, Zhejiang University, Hangzhou,
China
[b]School of Chemistry, Physics, and Mechanical Engineering Queensland
University of Technology Brisbane, QLD 4000, Australia

* E-mail: yhou@zju.edu.cn;

Experimental section.

Synthesis of EG foil. Graphite was rinsed with water, acetone and ethanol under sonication respectively, and then dried at 60 °C for 2 h. The EG was obtained by electrochemical exfoliation treatment of graphite foil in 0.1 M $(NH_4)_2SO_4$ solution at 10 V for 3 min.

Synthesis of EG/$Co(OH)_2$. EG/$Co(OH)_2$ was synthesized in a typical three-electrode system. The EG acted as working electrode and Pt foil acted as counter electrode, with reference electrode of Ag/AgCl electrode. The electrolyte was 0.05 M $Co(NO_3)_2$ solution. The chronoamperometric (-1.2 V vs. Ag/AgCl) technique was applied to electrodeposit the $Co(OH)_2$ nanosheets array on the surface of EG. After 150 s reaction, the EG/$Co(OH)_2$ was taken out and followed by washing with water. The as-prepared EG/$Co(OH)_2$ was further dried at 60 °C for 2 h, and a piece of cyan EG/$Co(OH)_2$ was obtained.

Synthesis of EG/$Co(OH)_2$/ZIF-67 hybrid. The EG/$Co(OH)_2$/ZIF-67 hybrid was prepared by a vapor-phase hydrothermal strategy. The EG/$Co(OH)_2$ was supported with a Teflon pillar on the back, and then the EG/$Co(OH)_2$/Teflon pillar together with 2-methylimidazole solution was placed into an PTFE autoclave. The autoclave was maintained 150 °C for different reaction times (5, 10, 15, 20, 30, and 40 min). During the process, 2-methylimidazole was heated and sublimated into the vapor. The $Co(OH)_2$ nanosheets array of the EG/$Co(OH)_2$ reacted with the 2-methylimidazole vapor, resulting in the formation of EG/$Co(OH)_2$/ZIF-67.

Characterization.

The microscopic morphology of the samples was observed by the field-emission scanning electron microscope (FESEM, Hitachi SU-8010) and transmission electron microscope (JEM-2100F). The element composition was analyzed by the energy-dispersive X-ray spectroscopy (EDX) analyzer (Oxford X-max80), which was combined with the FESEM. X-ray diffraction (XRD) test was carried out with X-pert Powder, PANalytical B.V. Considering the EG foil has strong diffraction peaks that can hide other peaks from ZIF-67 and $Co(OH)_2$ nanosheets, XRD patterns of samples were recorded by testing the powders collected from the surface of the EG based samples. Raman spectra were measured with a LabRAM HR Evolution and the X-ray photoelectron spectroscopy (XPS) was carried out on Thermo Fisher Scientific, Escalab 250Xi with Al Ka radiation. The contact wetting angle was photographed on the OCA20, and Fourier transform infrared spectra (FTIR) were recorded by the NICOLET 6700 FT-IR spectrometer. Atomic force microscopy (AFM) was performed on MultiMode 8.

Electrochemical measurements

All electrochemical measurements were carried out on an electrochemical analyzer (CHI 760 E, Shanghai) with a typical three-electrode cell where a Pt foil worked as counter electrode and an Ag/AgCl electrode worked as reference electrode. The electrolyte was 1.0 M KOH solution, and the reference was converted to reversible hydrogen electrode (RHE) via the Nernst equation ($E_{RHE} = E_{Ag/Ag/Cl} + 0.059 \times pH + 0.197$). As a part of the pretreatment, the cyclic voltammetry (CV) was scanned to stabilize the working electrode until the CV curves almost coincided. To get the polarization curve, linear sweep voltammetry (LSV) with a scan rate of 5 mV s^{-1} was performed. The durability test was carried out by both the chronoamperometric and chronopotentiometric methods, and the multi-current curve was recorded by the chronoamperometric method. The frequency range of electrochemical impedance spectroscopy (EIS) was from 100 K to 0.01 Hz, and the AC amplitude was 10 mV. All polarization curves were calibrated with iR correction.

The way to execute iR correction is based on the equation: $E = E_0 - iR$ Where E (unit V) is the potential after correction at the current of i (unit A), E_0 (unit V) is the potential data read from the polarization curves, i is the current at E_0 from the polarization curves, R (unit ohm) is the resistance obtained from the EIS result.

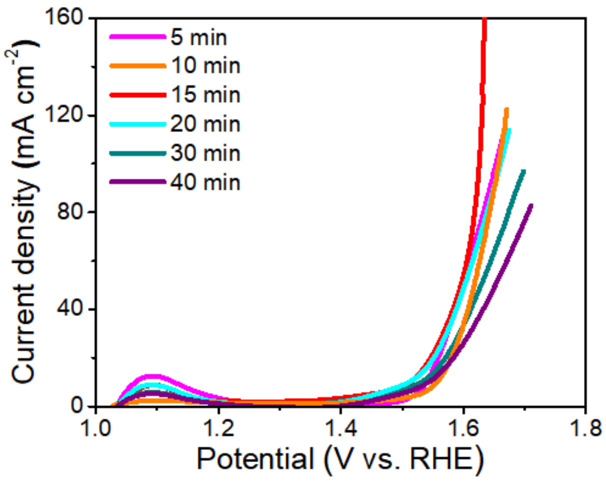

Figure S1. Polarization curves of EG/$Co(OH)_2$/ZIF-67 hybrid with different reaction time of 5, 10, 15, 20, 30, and 40 min.

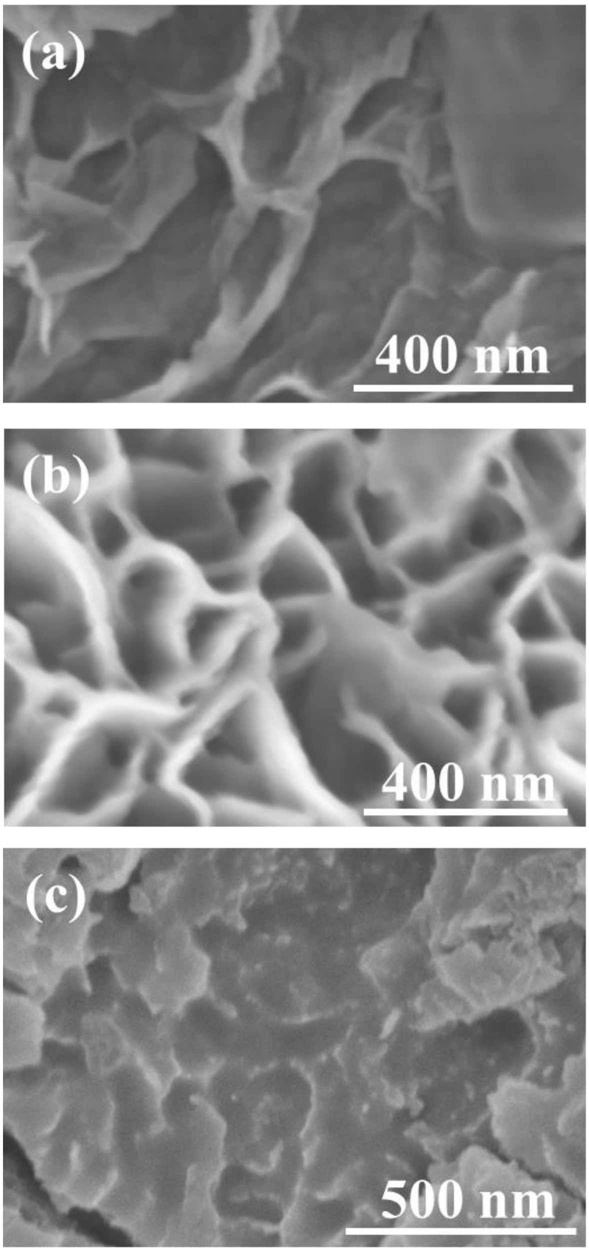

Figure S2. (a-c) FESEM images of EG/Co(OH)$_2$, EG/Co(OH)$_2$/ZIF-67 hybrid with 5 min, and EG/Co(OH)$_2$/ZIF-67 hybrid with 30 min.

Figure S2 gives the FESEM images of EG/Co(OH)$_2$/ZIF-67 hybrid samples with different reaction times. It can be seen that the thickness of ZIF-67 nanosheets has a great influence on the OER performance (Figure S1). As for the EG/Co(OH)$_2$/ZIF-67 hybrid with 5 min, the thickness of ZIF-67 nanosheets was about 2 nm (Figure S2b). Figure S2c shows the FESEM image of EG/Co(OH)$_2$/ZIF-67 hybrid with 30 min. The morphology of EG/Co(OH)$_2$/ZIF-67 hybrid changed from the nanosheets to clusters, and the OER performance of EG/$Co(OH)_2$/ZIF-67 hybrid with 30 min was much lower than that of EG/$Co(OH)_2$/ZIF-67 hybrid (Figure S1). This result indicates that a proper thickness of ultrathin ZIF-67 grown on the EG/$Co(OH)_2$ nanosheets could lead to a robust synergistic effect between ZIF-67 and $Co(OH)_2$, which could efficiently boost OER performance.

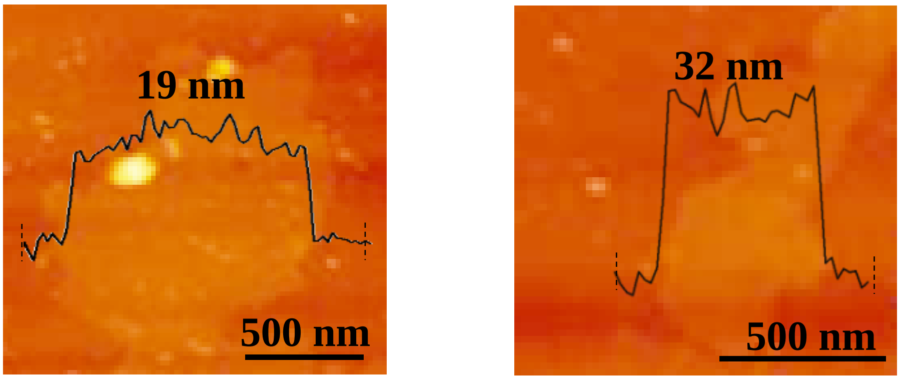

Figure S3. AFM images of EG/$Co(OH)_2$ and EG/$Co(OH)_2$/ZIF-67.

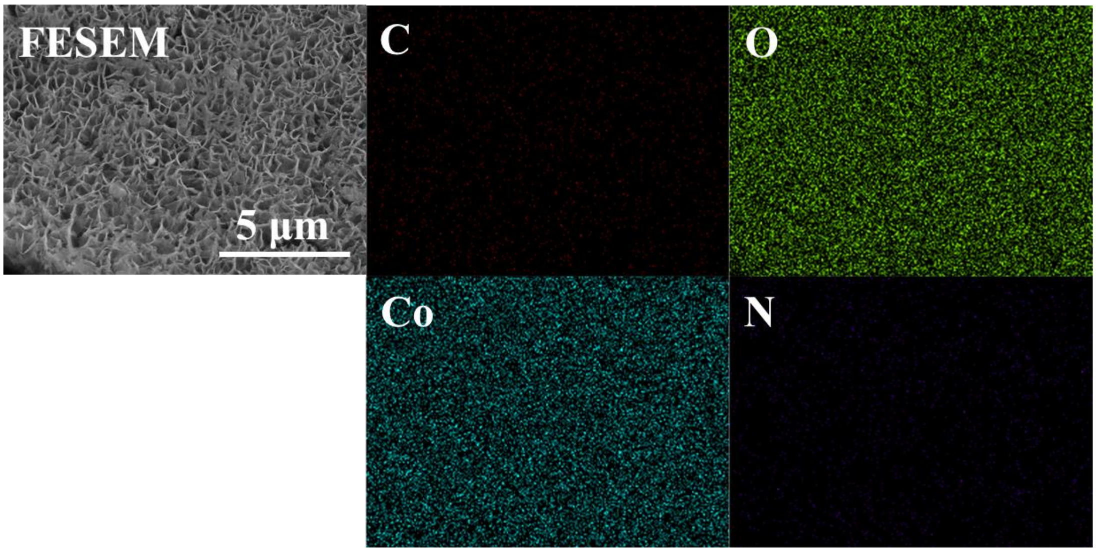

Figure S4. FESEM image and corresponding EDX mapping of EG/$Co(OH)_2$/ZIF-67 hybrid.

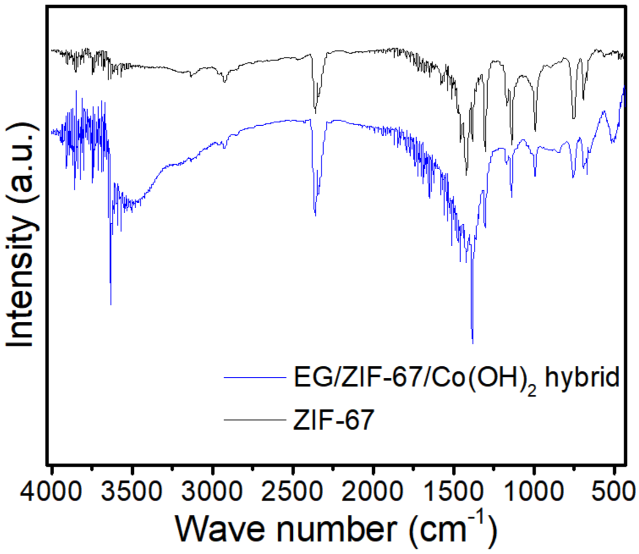

Figure S5. FTIR spectra of ZIF-67 and EG/Co(OH)$_2$/ZIF-67 hybrid.

As shown in Figure S5, the FTIR spectrum of EG/Co(OH)$_2$/ZIF-67 hybrid is similar with that of ZIF-67, which indicates that the EG/Co(OH)$_2$/ZIF-67 hybrid is consisting of ZIF-67. Moreover, the peaks at 510 cm^{-1} (stretching vibration of Co-O) and 3,630 cm^{-1} (stretching vibration of O-H) can be observed in the EG/Co(OH)$_2$/ZIF-67 hybrid, indicating the existence of Co(OH)$_2$ nanosheets.

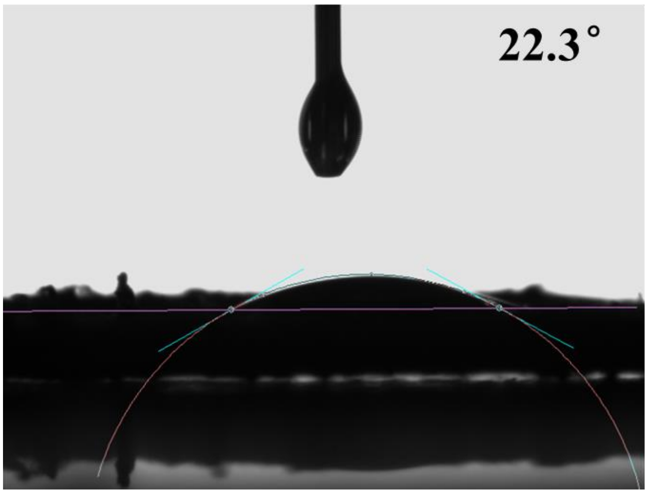

Figure S6. Contact wetting angle of EG/$Co(OH)_2$/ZIF-67 hybrid.

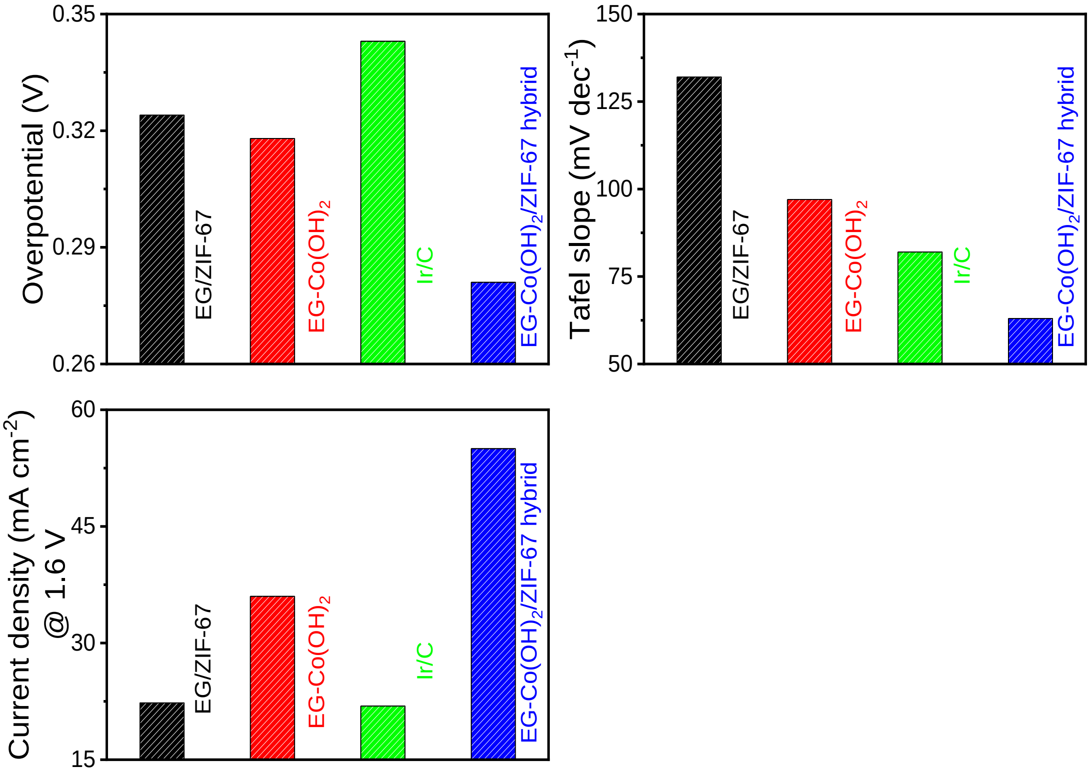

Figure S7. Overpotentials at 10 mA cm^{-2}, Tafel slope plots, and current densities at 1.6 V for EG/ZIF-67, EG/$Co(OH)_2$, EG/$Co(OH)_2$/ZIF-67, and Ir/C electrodes.

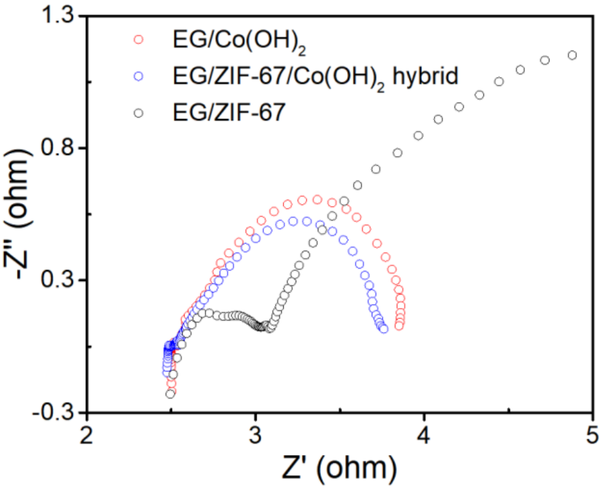

Figure S8. EIS plots of EG/ZIF-67, EG/Co(OH)$_2$, and EG/Co(OH)$_2$/ZIF-67 hybrid. The resistance of EG/Co(OH)$_2$/ZIF-67 hybrid is the lowest among the three samples.

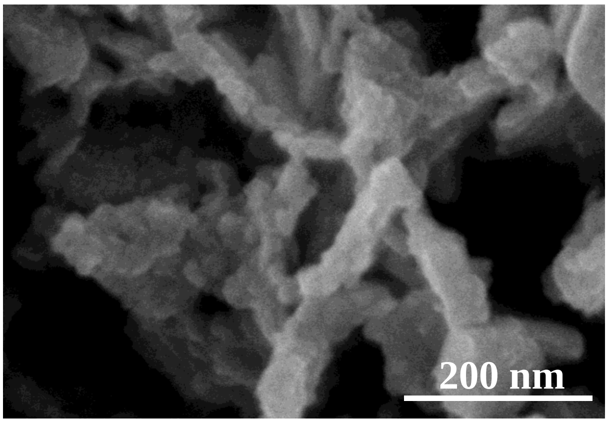

Figure S9. FESEM image of EG/Co(OH)$_2$/ZIF-67 hybrid after OER test.

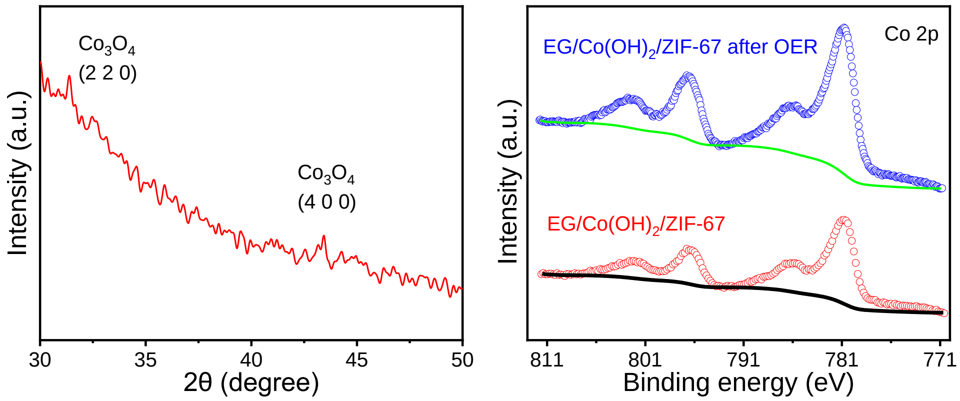

Figure S10. XRD pattern and high-resolution Co 2p spectrum of EG/Co(OH)$_2$/ZIF-67 hybrid after OER tests.

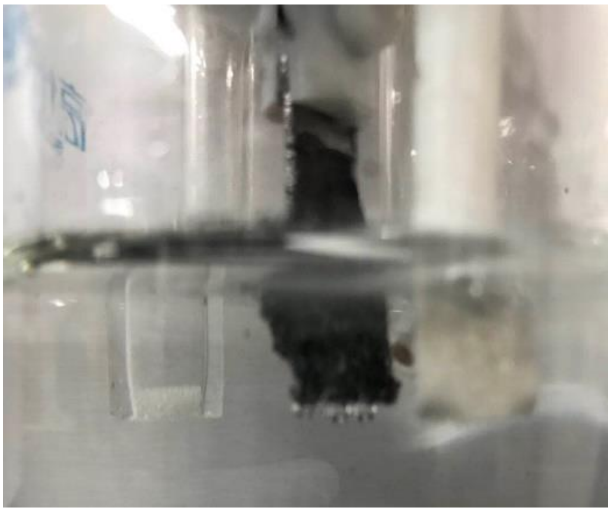

Figure S11. Digital photo of O_2 bubbles on the surface of EG/Co(OH)$_2$/ZIF-67 hybrid during the OER test.

Figure S12. Solar-driven water splitting process using the EG/Co(OH)$_2$/ZIF-67 hybrid.

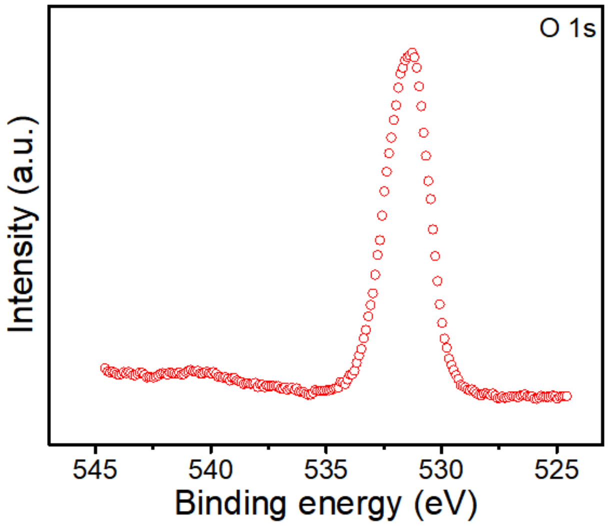

Figure S13. The high-resolution of O 1s XPS spectrum of EG/Co(OH)$_2$/ZIF-67 hybrid.

The high-resolution of N 1s XPS spectra of EG/Co(OH)$_2$/ZIF-67 hybrid given as Figure 5a show that the N exists in three formations, including pyridinic N at 398.4 eV, Co-N at 399.2 eV, and graphitic N at 400.2 eV, respectively.

The high-resolution Co 2p XPS spectra of EG/Co(OH)$_2$/ZIF-67 hybrid given in Figure 5b illustrate that the Co exists both in +2 and +3 states with their corresponding satellite peaks. The Co^{2+} 2p$_{3/2}$, Co^{2+} 2p$_{1/2}$, Co^{3+} 2p$_{3/2}$, and Co^{3+} 2p$_{1/2}$ peaks are located at 782.2, 797.2, 780.6, and 795.9 eV respectively. The strong coupling effect can be observed from the XPS spectra of N 1s and Co 2p XPS spectra (Figure 5a-5b). Notice the pyridinic N peak in the ZIF-67 is located at 398.6 eV, which is slightly higher than the position of pyridinic N peak in the hybrid (398.4 eV).

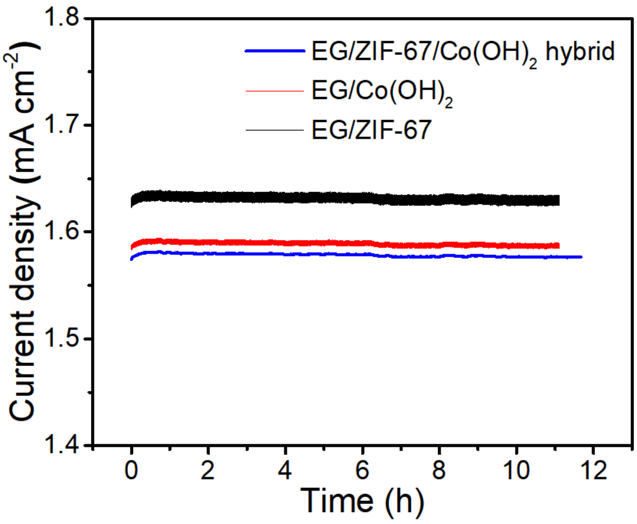

Figure S14. Chronoamperometric measurements of EG/ZIF-67, EG/Co(OH)$_2$, and EG/Co(OH)$_2$/ZIF-67 hybrid.

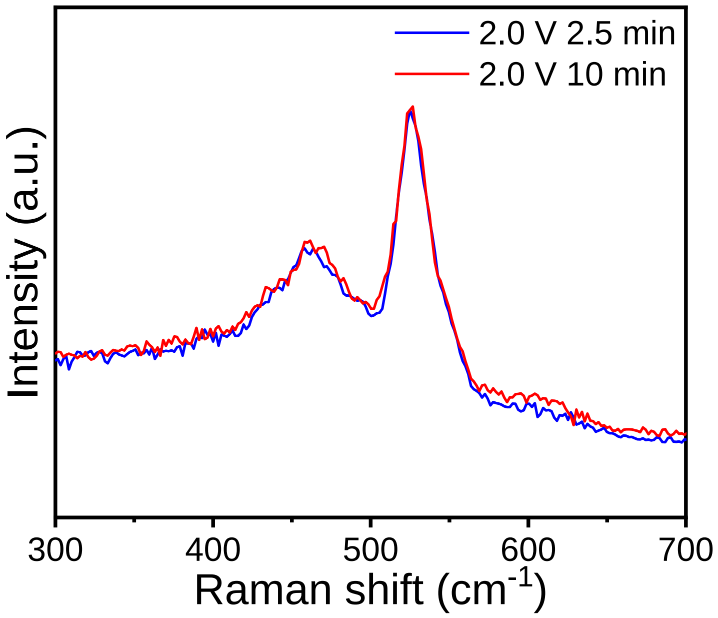

Figure S15. *In-situ* Raman spectra of EG/Co(OH)$_2$/ZIF-67 at 2.0 V for 2.5 min and EG/Co(OH)$_2$/ZIF-67 at 2.0 V for 10 min.

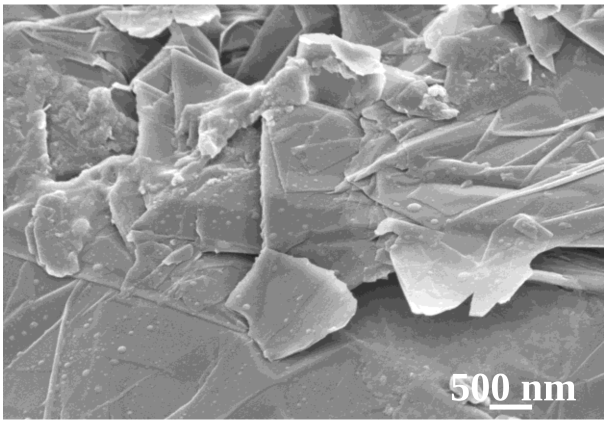

Figure S16. FESEM image of exfoliated graphite foil.

Table S1. Comparison of OER performance of EG/$Co(OH)_2$/ZIF-67 hybrid with those representative ZIFs based OER electrocatalysts.

Author	Catalyst	Current density J	Potential at the corresponding J (vs. RHE)	Electrolyte
This work	**EG/$Co(OH)_2$/ZIF-67 hybrid**	**10 mA cm^{-2}**	**1.51 V**	**1 M KOH**
Nat. Energy 2016, 1, 15006	N-doped carbon nanotube	10 mA cm^{-2}	1.60 V	1 M KOH
ACS Appl. Mater. Interfaces 2017, 9, 7193	UTSA-16	10 mA cm^{-2}	1.64 V	1 M KOH
Adv. Funct. Mater. 2017, 27, 1606497	PPy/FeTCPP/Co	10 mA cm^{-2}	1.57 V	0.1 M KOH
ACS Appl. Mater. Interfaces 2017, 9, 37548	CoCd-BNN	10 mA cm^{-2}	1.58 V	0.1 M KOH
Nano Energy 41 (2017) 417	CUMSs-ZIF-67	10 mA cm^{-2}	1.54 V	1 M KOH
Nano Energy 45 (2018) 127	PANI/ZIF-67	10 mA cm^{-2}	1.56 V	0.1M KOH
J. Mater. Chem. A, 2018, 6, 1188	NiPc–MOF	10 mA cm^{-2}	1.48 V	0.1 M KOH
Electrochimica Acta 219 (2016) 623	Ti@TiO_2/CdS/ZIF-67	10 mA cm^{-2}	1.64 V	1 M NaOH

Adv. Funct. Mater. 2018, 28, 1704638	Co–N_x/C NRA	10 mA cm^{-2}	1.53 V	0.1 M KOH
J. Mater. Chem. A, 2018, 6, 5999	Co-LDHNS	10 mA cm^{-2}	1.57 V	1 M KOH